13th International Conference on
Structural Health Monitoring of Intelligent Infrastructure
DOI: 10.3217/978-3-99161-057-1-100

Integrated Sensor Technology for Basalt-Reinforced Segmental Lining Elements

Alexandros Evangelatos[1, ORCID 0009-0000-7300-1686], Lukas Heindler[2, ORCID 0000-0003-3951-8838], Robert Galler[1, ORCID 0000-0002-1150-4525], Thomas Thurner[2, ORCID 0000-0003-3783-1193]
[1]Department Mineral Resources Engineering, Chair of Subsurface Engineering,
Montanuniversität Leoben, Erzherzog-Johann-Straße 3/III, 8700 Leoben, Austria
[2]Department Product Engineering, Chair of Automation and Measurement,
Montanuniversität Leoben, Peter-Tunner-Straße 25/II, 8700 Leoben, Austria
email: alexandros.evangelatos@unileoben.ac.at, lukas.heindler@unileoben.ac.at

ABSTRACT
Current climate protection goals are driving research toward large-scale structural health monitoring solutions for critical, long-lifespan infrastructure, alongside the usage of low CO_2 emission materials. In this work, we present an innovative approach that combines both aspects: the use of continuous basalt fibers assembled into sustainable reinforcement structures, and low-cost measurement systems for integrated long-term condition monitoring, specifically applied to tunnel segment monitoring. As a proof-of-concept for the integration of sensor elements into basalt reinforced concrete structures, we utilized stranded steel wire to create custom strain gauge sensors for integrated strain measurements, paired with a custom-designed resistive bridge-based measurement system to evaluate the feasibility of enabling low-cost condition monitoring. Mechanical tests were conducted on basalt-reinforced concrete specimens under both tensile and compressive loading. The results indicate that the system can measure even low strain values for the sensor-enhanced structures down to approximately 5 µm/m and a standard deviation of 2.1 µm/m, achieving a sensing performance close to state-of-the-art measurement systems and externally applied standard strain gauges. The study demonstrates the potential for cost-effective condition monitoring of individual tunnel segments with sustainable basalt reinforcement. Further optimizations of the system are anticipated in future projects.

KEY WORDS: Structural health monitoring; Strain measurements; Integrated stress monitoring; Crack detection; Basalt fiber reinforcement; Tunnel segment monitoring; Segmental lining element; Measurement system design; Low-cost electronics.

1 INTRODUCTION

The expansion of the European infrastructure network and the growth of international metropolises are increasing the need for major road and railway construction projects. Tunnelling and bridge construction are essential in this context. At the same time, the focus is shifting to climate protection and ambitious international targets. According to the Climate Act, the EU is committed to reducing net greenhouse gas emissions by 55% by 2030 and becoming climate-neutral by 2050 [1].

The construction and building sector is responsible for 38% of global CO_2 emissions and harbors great potential for innovation [2]. Cement production alone contributes 3.3% to Austria's and 4.5% to global emissions [3][4].

Structural steel in reinforced concrete is approx. 3 to 5 times more CO_2-intensive per ton. According to a study on the Brenner Base Tunnel, one ton of structural steel emits 1,980 kg of CO_2, while cement emits 576-622 kg of CO_2 per ton [5][6]. In segmental lining elements, concrete can contain approximately 150 kilograms of steel per cubic meter. The production of 150 kilograms of steel emits nearly the same amount of carbon dioxide as the cubic meter of concrete surrounding it. Consequently, a low-CO_2 material as an alternative to steel reinforcement offers great sustainability potential.

Due to these challenges, ongoing research projects are investigating the use of basalt fibers as a sustainable alternative for concrete reinforcement. The key advantages include significantly lower production intensity and CO_2 emissions compared to steel, as well as high corrosion resistance. Other beneficial properties include higher tensile strength than steel, low weight, and fire resistance. Additionally, basalt reinforcement exhibits electrically insulating characteristics, resulting in longer lifespans of basalt-reinforced materials [7].

While the application of basalt fibers is also being researched in the form of macrofibers, this study considers continuous fibers with diameters of 17 µm ± 1 µm [8] bundled into multifilament yarns. These fibers can resemble structural steel in the form of Basalt fiber-reinforced polymer (BFRP) rebars or be woven into grid-like structures. Due to their processability, they can also be woven into 3D structures and precisely manufactured to meet specific load-bearing requirements. To maintain the stability of the reinforcement structure and ensure the stress distribution among the individual filaments within the bundle, they are impregnated with resin [9].

The manufacturing method allows for the processing of various fiber materials, leading to the concept of integrating a sensing fiber for strain measurements. The precise placement of fibers during the process enables the defined integration of measurement sensors, ideally within a fully automated manufacturing setup. The process combines sustainable and corrosion-resistant basalt fiber reinforcement with an efficient method for structural health monitoring. This offers significant potential in saving CO_2 emissions, particularly relevant in tunneling, where the required structural service life often exceeds 100 years [10].

The production of reinforcement structures using basalt fibers is considered to be particularly advantageous for prefabricated construction [7], placing the focus of our investigations on segmental lining elements. By equipping each

DOI: 10.3217/978-3-99161-057-1-100

segment with an integrated, low-cost measurement device, continuous structural health monitoring could be extended beyond individual rings to cover the entire tunnel, enabling comprehensive long-term condition assessment. Building on this approach, we have extended our research to include the development of a cost-effective measurement system. Figure 1 shows the conceptual sketch of the combined basalt reinforcement and integrated strain gauges in a tunnel segment.

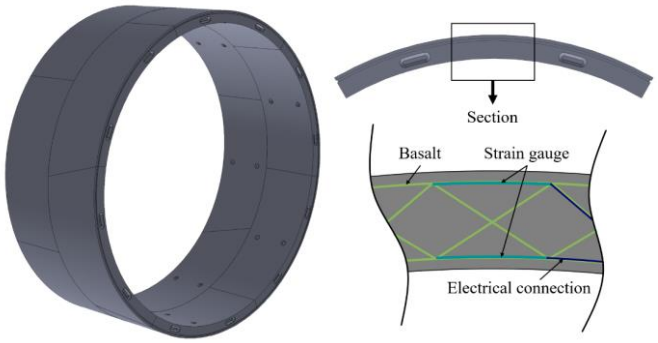

Figure 1. Segmental lining element ring and a conceptual sketch of the basalt reinforcement with integrated strain gauges in a tunnel segment.

The sensor's measuring length can be tailored to accommodate the desired spatial resolution and range. The strain sensor's integration into the reinforcement windings ensures precise measurement along the axis of maximum force, resulting in optimal measurement signals. An overlapping sensor configuration with varying measuring lengths is being evaluated for localized crack detection.

2 STATE OF THE ART METHODS

Current methods for ensuring structural safety and functional maintenance of tunnels rely on regular inspections. A distinction is made between destructive methods, core drilling, and non-destructive methods for condition monitoring.

The Austrian Federal Railways (ÖBB), for example, governs these inspections by the RW 06.01.02 regulations [11], focusing on crack formations in the tunnel linings. Tunnel scanners are used to create high-resolution images of the inner shell surface. Despite ongoing artificial intelligence integration, the process remains labor-intensive due to specialized equipment and manual evaluation [12][13].

In addition to condition assessments conducted through inspections, systems for continuous long-term monitoring (LTM) and structural health monitoring (SHM) are also employed. One focus is geotechnical monitoring, for which instrumentation, typically comprising extensometers, pressure cells, and convergence systems [14], are strategically installed in areas where geologically unstable zones, such as fault zones and swelling rock formations, are anticipated. The systems can be installed deep within the surrounding rock mass, extending behind the structural construction, in order to record data from the unaffected or stable rock formations.

To monitor the stress state of concrete structures, measurement systems are commonly embedded within the concrete matrix. These systems are typically attached to the reinforcement to ensure precise positioning, or alternatively, they are mounted to separate structural elements, particularly in the case of unreinforced concrete. The two most common systems for SHM in tunnelling are based on strain gauges (SG) and distributed fiber optic sensing (DFOS). Both sensor types are applied in cast-in-place concrete, such as inner linings, as well as in precast elements, such as tunnel segments.

Vibrating wire sensors provide accurate measurement of strain and, consequently, allow for analytical prediction of stress within the tunnel lining. However, they are limited in their strain length, often below 250 mm. Therefore, they only provide localized data from a few selected points. Furthermore, data is manually collected on-site from individual measurement boxes, which often require road enclosures.

The more recent advancement in SHM with DFOS offers several benefits over SGs. One fiber optic cable enables multiple measurement points within the structural component, making it an ideal system for crack detection [15]. Additionally, data transmission can be performed over long distances without significant loss, allowing the measurement analysis to be conducted outside the tunnel. However, DFOS systems require careful installation and protective measures to ensure durability. To enhance robustness, they are often encased in a thick protective layer, compromising flexibility and being subject to strain incompatibilities with the material to be monitored. The complex setup and costly instrumentation are key reasons for the installation at only few locations [16].

An innovative alternative to conventional monitoring methods involves using carbon fiber reinforcement not only for structural support but also as a sensor [17]. Although carbon fibers offer greater durability and tensile strength, they are far less favorable than basalt fibers in terms of CO_2 emissions during production, production costs and handling during installation [7].

The presented disadvantages of the existing solutions speak in favor of the approach pursued in this work of a sensor system that can be fully and automatically integrated into the basalt reinforcement structure. This cost-efficient approach enables continuous SHM not only of sections, but the entire tunnel. A holistic SHM system is essential for detecting overstressing early, thereby enhancing safety, minimizing downtime of infrastructure, and reducing overall maintenance costs [12]. Particularly relevant for infrastructures such as tunnels with a projected and required long service life.

3 METHODOLOGY

Current state-of-the-art metrology solutions to measure strain on tunnel segments, like DFOS, offer precise measurement data and can, therefore, reliably monitor the few segments in which they are integrated. With this approach, the condition of other segments can only be estimated. Reliable condition monitoring of the whole tunnel system, however, depends on the condition monitoring of each segment. Therefore, more cost-effective and simpler solutions must be used. The following sections cover metrology, and the electronics used for this goal.

The Methodology section is divided into several subsections. It begins with the sensor conceptualization and the description of the hand-patterned steel wire strain gauge used in the devices under test. Next, the construction of the test device is discussed, including the design of the specimen. Following this, the

DOI: 10.3217/978-3-99161-057-1-100

subsequent subsection describes the design of the custom electronic measurement system and the theoretical measurement principle behind the approach. In the final subsection, the test procedures that were conducted are explained.

3.1 Sensor Concept

Readily available strain gauges suitable for condition monitoring of tunnel segments are expensive and challenging to mount automated and securely on reinforcement or concrete surfaces. Additionally, the precise location and orientation of the strain gauges may become uncertain if they shift during the concrete pour. A more practical approach would involve integrating the strain gauges into the construction of the concrete reinforcement. One potential method involves integrating a resistance wire into the basalt reinforcement fabrication at predefined areas of interest and measuring the reinforcement's strain at those locations. This process can be automated using existing robots, simplifying the integration process. Prototype devices discussed in this work are equipped with hand-wound strain gauges glued to the basalt reinforcement. In future production processes, the resistance wire would be integrated between individual strands of the prefabricated basalt reinforcement of a concrete segment.

Accompanying electronics would need to be attached during this process. After concrete pouring and electronic verification, the segment would be ready for mounting inside a tunnel.

Because the anticipated operation duration is several years to decades, common issues such as creep and sensor degradation can affect long-term strain measurements. This may lead to false-positive or false-negative alerts regarding damage in the tunnel segment. These factors are a significant focus of our research and pose major concerns for the design and development of our condition monitoring system.

In this work, a stranded steel wire with 90 strands and a diameter of 14 µm per strand is used. Electrical insulation between each winding is guaranteed due to the careful forming of meanders by hand. The specific resistance is approximately 70 Ω/m. 1.74 meters of wire are used, which results in 120 Ω resistance, accommodating standard bridge measurement systems.

The steel wire exhibits a gauge factor k of approximately 2, a typical value for metal strain gauges [18][19]. The gauge factor relation k is defined by

$$k = \frac{\Delta R/R_0}{\Delta l/l_0} = \frac{\Delta R/R_0}{\varepsilon} \approx 2 \ . \qquad (1)$$

In the given equation the gauge factor k is defined as the ratio of the relative change in electrical resistance $\Delta R/R_0$ to the technical strain ε. The strain ε is given by the relative elongation, where Δl is the change in length and l_0 is the initial length. Similarly, ΔR denotes the change in electrical resistance, while R_0 is the initial resistance of approximately 120 Ω.

For clarity, relevant values of the steel wire material are presented in Table 1, the wire is a Bekinox® VN-fiber 14.1.9 from Bekaert [20]. The stainless-steel fiber bundle was chosen as the sensor material due to its corrosion resistance and the fact that the strands are not twisted. The individual strands are held together by a limited number of wrapped polyester filaments.

Table 1. Test strain gauge properties. [20]

Steel fiber: Bekaert Bekinox® VN-fiber 14.1.9			
Diameter	Strands	Ω/m	k-factor
14 µm	90	70	2

Before concrete pouring and after curing, a digital multimeter was used to measure the wire's resistance and ensure proper installation and electrical connection.

3.2 Test Device Construction

Prior to the concrete tests, tensile tests using PET film were conducted to validate the measurement concept. The steel wire was mounted to a PET film strip over an approximate gauge length of 120 mm with seven meanders, using an epoxy adhesive. To verify the measurements, an additional reference strain gauge with the same length was attached adjacent. The promising results obtained justified further investigations in the context of the intended application on basalt reinforcements.

In the subsequent tests, the steel wire was attached by hand to the basalt rods using epoxy. Two types of reinforcement were used: basalt rebars with a diameter of 8 mm [21] and custom-manufactured basalt rods. The latter consisted of a total of 16 basalt fibers, each with a linear density of 2400 tex [8], bundled together. The 16-fiber configuration closely approximates the cross-sectional area of the basalt rebar and is intended to resemble the future application of fully automated placement of continuous basalt fibers into 3D reinforcement structures.

Figure 2 shows the steel wire strain gauge conceptual drawing and a BFRP rebar with the steel wire attached to the surface with epoxy, after a destructive compressive test.

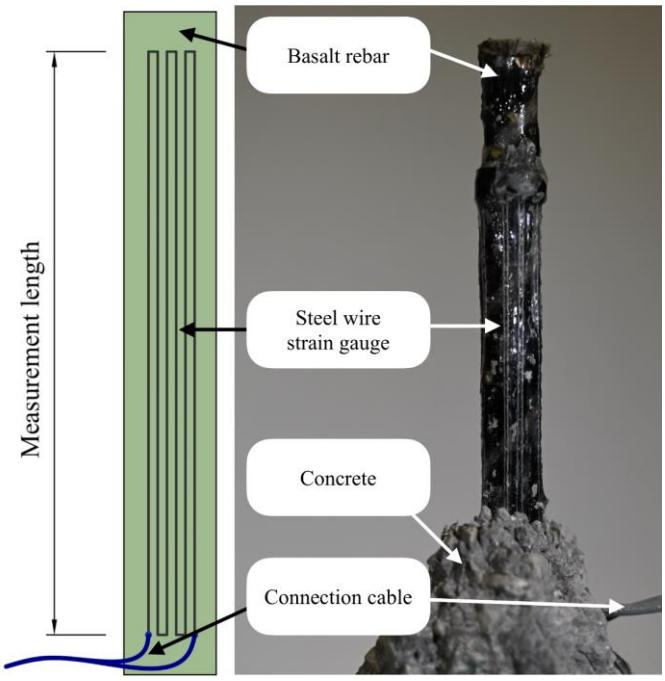

Figure 2. Steel wire strain gauge conceptual drawing and implementation on basalt-reinforced polymer rebar after destructive compressive test.

DOI: 10.3217/978-3-99161-057-1-100

Due to the small test geometry, multiple meanders were required. After the test, pieces of concrete were additionally detached for inspection of the steel wire.

Two test arrangements were designed for both basalt materials, with only one basalt rod in the center of each specimen, to investigate the suitability of the test strain gauge applied to basalt reinforcement inside concrete elements. The designs were developed to account for the different directions of applied force or load, specifically in both tension and compression directions. Both concrete specimen designs are cylindrical with only one reinforcing basalt rod in the center. The dimensions of both designs can be viewed in Figure 3. PVC pipes were used as molds for the concreting process. The concrete mix of both designs was similar to typical formulations used in precast elements for tunnel construction.

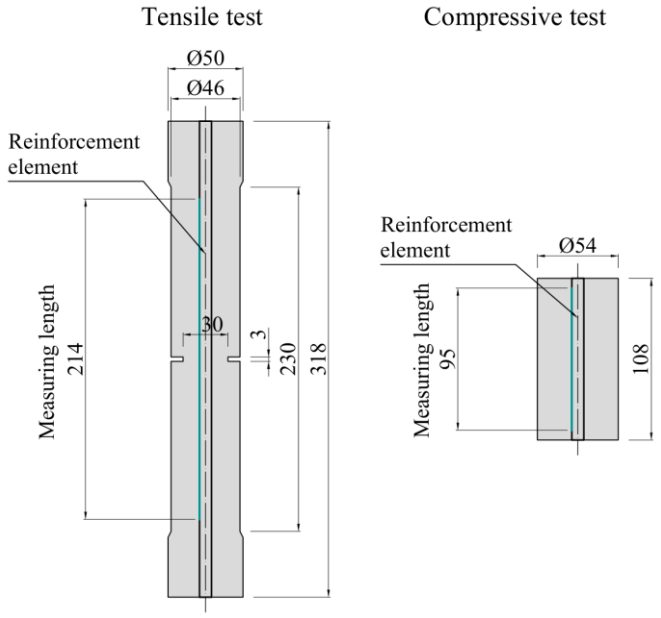

Figure 3. Specimen geometry for tensile (left) and compressive tests (right) with measuring length (in mm) and strain gauge (blue) on basalt reinforcement element.

The concrete mix design originates from the corresponding specification for precast tunnel segments but was adapted to suit the test specimen size. Specifically, aggregate fractions exceeding 8 mm were excluded and their mass proportions were redistributed among the other grain sizes. The cement used was CEM I 42.5 R-SR, and Dynamon NRG 1010 NK was employed as the superplasticizer and accelerator. Due to the slender design, the concrete was poured in layers with intermittent short compaction cycles on a vibrating table to minimize the formation of large pore spaces. Additionally, unreinforced specimens were produced for each mixing batch to determine the uniaxial compressive strength (UCS).

After demolding the tensile specimens, they were further modified by a 3 mm wide and 8 mm deep notch, achieved through four cuts with a stone saw, to ensure the formation of a central crack during the destructive tensile test. The central crack formation enables comparability of the strain gauges, as cracks near the fixtures, for instance, could occur outside the shorter measurement range of the reference strain gauge.

Due to the required length of the resistive sensor element of approximately 1.74 m to achieve a resistance of approximately 120 Ω, suitable for the commercially available bridge measurement devices, the steel wire test strain gauge had to be arranged in a meander pattern, resulting in varying effective gauge lengths between the tensile and compression tests. As a reference, a commercial strain gauge from the company Althen BV was applied to the outer surface of the concrete specimen after demolding. Two reference strain gauge types for concrete, mortar, and rock materials were applied: PL-120-11-3LJCT-F and PL-60-11-3LJCT-F. Both types feature a three-wire parallel vinyl cable configuration in a three-wire quarter-bridge setup [22]. The reference strain gauges were mounted on the surface with a 120 mm measuring length on the tensile and 60 mm on the compressive specimens, intended for the comparison of the inner strain on the basalt reinforcement to the strain on the outer concrete surface.

The specific steel wire gauge lengths and the required number of meanders for each test configuration was adjusted to the specimen length. For the tensile test setup, the measuring length was set to 214 mm with 4 meanders on the basalt reinforcement. The shorter compressive tests required 9 meanders of steel wire over the measuring length of 95 mm.

3.3 Electronic Design

The strain gauges' resistance is commonly not directly measured but rather utilized in a resistance measurement bridge. Therefore, a quarter bridge measurement to determine the strain of the specimen under test using the approximated strain relation presented in Equation (2) was used:

$$\varepsilon \approx \frac{4 \cdot V_d}{k \cdot V_0} \tag{2}$$

Here, V_d represents the amplified differential voltage of the two bridge arms, k is the gauge factor of the strain gauge, and V_0 denotes the excitation voltage applied to the Wheatstone bridge.

As state-of-the-art measurement tools prove to be impractical for large-scale tunnel condition monitoring, a complementary, low-power, and compact electronic measurement system approach is being tested throughout the measurements. The block diagram of the developed prototype electronics is presented in Figure 4.

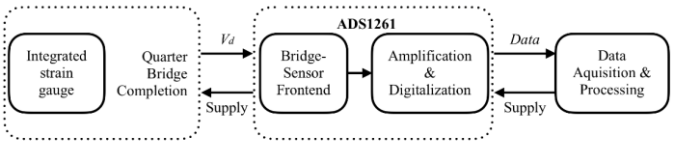

Figure 4. Block diagram of the developed measurement system. The device under test is employed in a quarter bridge. The ADS1261 IC measures the bridge voltage V_d and supplies the bridge with its internal voltage reference. An Arduino Uno R4 Minima reads the digitized data. Additionally, the Arduino exports its data to a PC for data storage.

The primary focus of this design is the sensor front-end section. This part is responsible for analog-to-digital conversion, amplification, filtering, and transmission of the digitized measured bridge voltage V_d. Furthermore, the resistance bridge must be supplied either by a current for absolute resistance changes or a voltage source for relative resistance changes. In addition to signal conditioning, the sensor front-end must

DOI: 10.3217/978-3-99161-057-1-100

communicate with a microcontroller to transmit the measurement data to a PC for further signal processing. Given the significance of various key parameters, such as offset drift, linearity, potential supply outputs, the number of analog inputs, the number of samples per second, the possible integrated circuit (IC) supply ranges, package sizes, and recommended applications, the sensor front-end ADS1261 [23] (Texas Instruments, Inc.) was selected as the preferred choice. This sensor front-end incorporates a precision 40 kSPS Delta Sigma analog-to-digital converter (ΔΣ-ADC), along with a programmable gain amplifier (PGA), an internal precision voltage reference, and an internal current source for bridge applications. Furthermore, the ADS1261 provides programmable registers to configure sampling rates, 4-wire or 6-wire measurements, current or voltage-driven bridge supply, PGA gain, filter modes, and read-only registers for data transmission over the serial peripheral interface (SPI). For the initial prototype, an Arduino Uno R4 Minima [24] (Arduino, Inc.) was used to read-in the digitized bridge level data. For this purpose, an algorithm to configure the ADS1261 registers for a predefined operating mode and a voltage-driven bridge circuit was developed. It then read the incoming data and displayed it on the Arduino's serial monitor for further storage and processing.

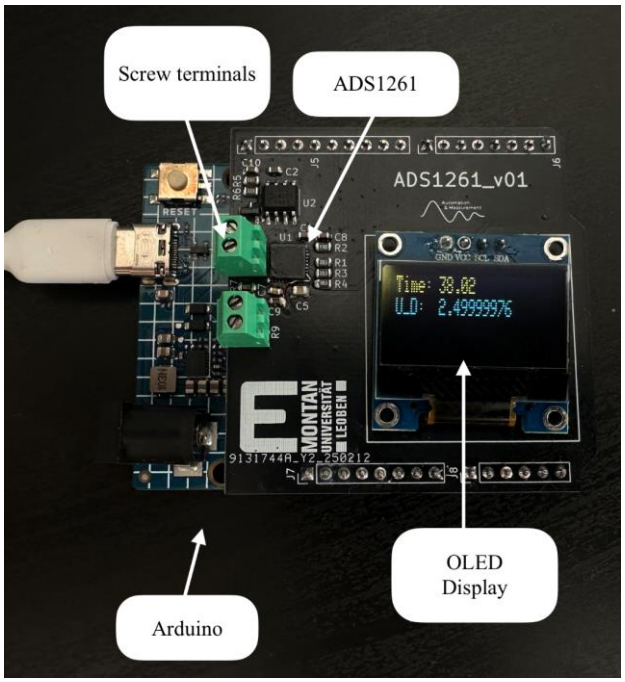

Figure 5. Developed Arduino shield incorporating the ADS1261 bridge front-end, screw terminals, and an OLED display for data visualization and debugging.

Furthermore, a printed circuit board (PCB) was designed and constructed. It integrates the ADS1261, connectors for the steel fiber strain gauge, and an OLED screen for data visualization, as shown in Figure 5. The printed circuit board was designed to fit seamlessly onto the Arduino pins, facilitating a direct connection. Such boards are commonly referred to as shields.

The strain gauge connection was realized with screw terminals as seen in light green and will be replaced by soldered connections in future revisions for a smaller contact resistance. These terminals form one half of the measurement bridge. This approach enabled adaptation for every strain gauge resistance within certain linearity boundaries. Given a specific strain gauge resistance, either two strain gauges can be connected to form a temperature-compensating half bridge, or a resistor with an equal no strain resistance can be connected to the second terminal to form a quarter bridge circuit.

3.4 Test Configurations

Building on the success of previous proof-of-concept measurements that involved creating a test strain gauge by attaching a steel wire to a plastic foil for tension tests, handcrafted concrete test devices are used for the following evaluations. These devices are equipped with handcrafted meander-shaped strain gauges and serve as preparatory tools for future tests involving real segmental lining elements.

Figure 6 depicts the setup comprising the devices under test for tensile and compressive tests in the test stand, including the load cell in the tensile test arrangement, and the mechanical measurement connections that can be applied as tensile force or compression force by a servo-hydraulic actuator.

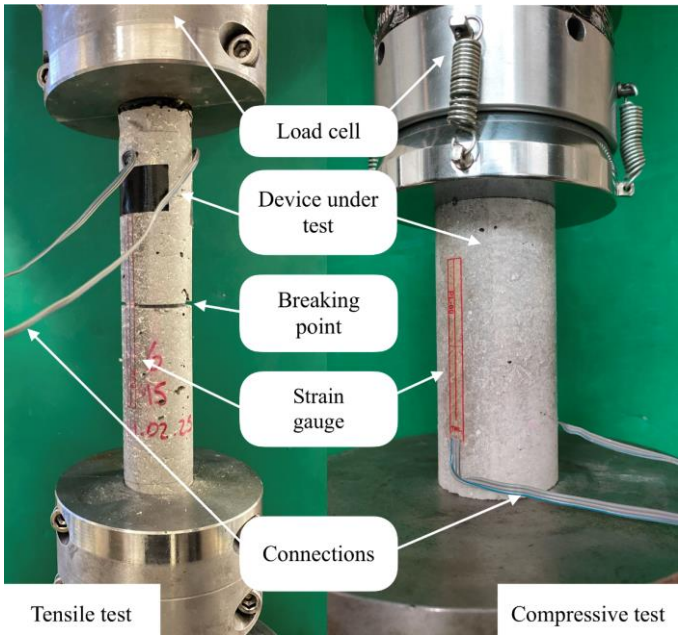

Figure 6. Test setup with the device under test mounted securely for tensile and compressive tests. Inside the device a steel fiber strain gauge is used. On the outside of the device, a standard strain gauge is installed. The load cell measures the applied force.

During measurements, the test stand applies and records force and travel distance in the longitudinal direction of the device under test. This force induces elongation or compression in the device and the strain gauges. Consequently, the strain gauges' resistances are anticipated to change. As a result, the strain/force relation can be quantified and visualized. As the resistance of the strain gauge also fluctuates in response to temperature, air pressure, magnetic field, and electromagnetic radiation changes, all of these factors were held constant to the extent practicable.

After constructing the devices under test and allowing a curing time of seven days, realistic test conditions were assumed. Special clamps to hold the devices, which are equipped with elastic rubber bands at the clamp edges were

DOI: 10.3217/978-3-99161-057-1-100

used to ensure equal pressure around the circumference of each device. Once the devices were mounted in the clamps, the connection wires to the measuring devices were connected. At this stage, a small amount of pre-tension or pre-compression was applied to ensure that the test stand can directly apply force during movement without any forceless travel.

Due to a limited number of test devices resulting from the tedious manufacturing process, several measurements using non-destructive forces with half of the expected maximum force before failure were conducted. This approach allowed us to measure strain with multiple setups before any devices were destroyed. The testing control paradigm varied between the two test setups. The compression test was conducted in force-controlled mode with a linear increase in applied force over time. In contrast, the tensile test was performed in distance-controlled mode by linearly increasing the distance between the mounting positions of the device under test, due to easier test stand programming.

As the final step of a measurement session, a destructive test was conducted. During destructive tests, the applied force exceeded the load-bearing capacity of the concrete, leading to the formation of cracks. In the case of the displacement-controlled tensile test, the applied force drops rapidly after the expected initial crack in the pre-notched specimen center. Further cracks form along the length of the specimen. Depending on the arrangement, different reactions occur at the inner and outer measuring areas.

Table 2. Relevant specimen and test parameters.

	Tensile	Compressive
Number of samples	6	3
Number of tests	25	13
Nondestructive force (kN)	1.5	45
Destructive force (kN)	4	120

The experimental test program on the steel wire strain gauge with basalt fiber-reinforcement materials is structured into tensile and compressive tests as presented in Table 2. The number of tests includes the number of repeated non-destructive variants and the final destructive ones for each test sample. Estimates of nondestructive and destructive loads are based on the results of tests with unreinforced concrete specimens.

4 RESULTS

Out of many test measurements, selected results based on their significance are presented in this section. Both for tensile and compressive tests on the reinforced concrete test objects, we present comparisons between the measurement signals recorded by a Quantum MX1615B [25] (HBK, Inc.) measurement system and the custom bridge measurement system. We organized the setups such that each strain gauge was measured with each measurement device, but for sequential and separate measurements. For instance, the inner strain gauge was connected to the MX1615B, and the outer strain gauge to the custom electronics during one non-destructive test. In the subsequent non- destructive test, we switch the connections. This method allows qualitative comparison of the results obtained by the MX1615B device and the results obtained by the custom electronics.

Using its accompanying software tool, we set a low-pass filter using a 4th-order Bessel filter, with a cutoff frequency of 10 Hz at a measurement rate of 50 Hz, for the Quantum MX1615B measurements.

For all signals recorded by the measurement systems, zero-phase digital filtering in the signal post-processing using Matlab's `filtfilt()` function was applied. In this case, an FIR low-pass filter with a cutoff frequency of 2 Hz and a length of 101 was implemented. This approach ensures no phase delays of different frequency compone nts of the measurement signal.

4.1 Tensile tests

Based on previous test measurements conducted with unreinforced concrete test specimens, non-destructive tensile tests were performed with estimated tensile forces below 1.5 kN, less than half of the expected maximum load, as stated in Table 2. Given the relatively small forces, only minor strains

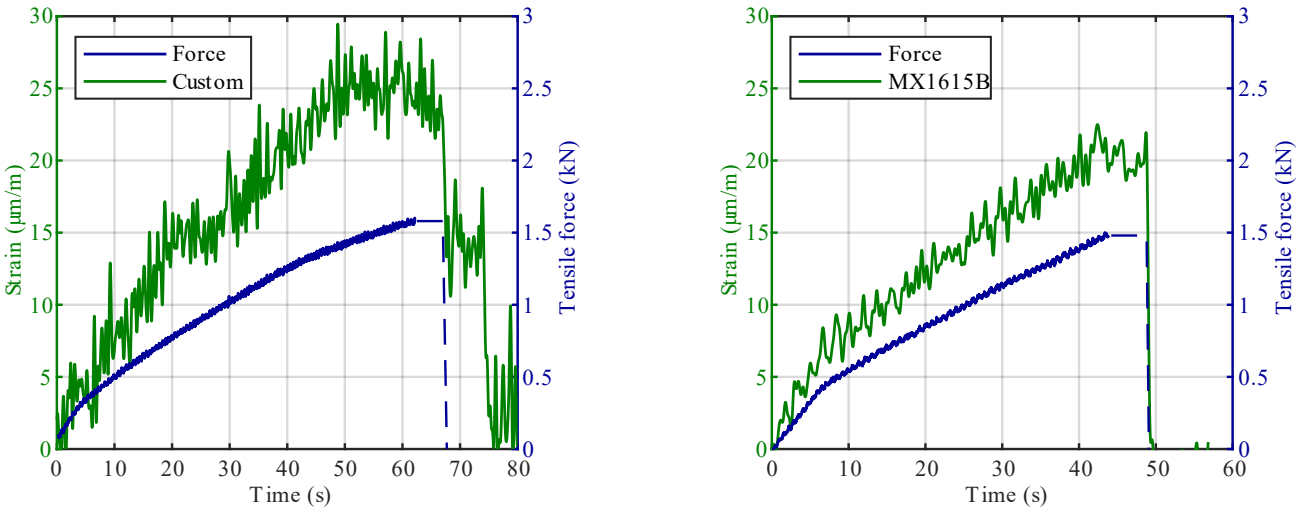

Figure 7. Two non-destructive tensile tests with an in-built hand-made strain gauge in green, measured with the custom-made electronics (left) and with the MX1615B (right). The applied tensile force is shown in blue.

DOI: 10.3217/978-3-99161-057-1-100

of less than 50 µm/m were anticipated, which was reflected by the executed measurements. Figure 7 shows two measurements of different test measurements using the same device under test for a qualitative comparison between the custom measurement system and the MX1615B. Each plot illustrates the tensile force resulting from uniform cylinder motion in blue and the low-pass filtered measurement signal from the measurement systems connected to the inner steel wire strain gauge in green. In the left plot, the measurement signal of the custom electronics is shown. On the right side, the measurement signal from the MX1615B instrument. Both measurement signals were digitally filtered with the aforementioned FIR low-pass filter with a filter length of 101 and a cut-off frequency of 2 Hz. As one can observe, at these strain values, even the reference measurement system MX1615B has significant signal variations.

Most non-destructive tensile tests were conducted over a duration exceeding 60 seconds, as the test stand exhibited a slow but consistent movement. It is evident from Figure 7 that the reduction of the tensile force signal precedes the end of the load sequence. The tests concluded at this point, and the force was set to zero manually after a few seconds, shown with the dashed blue line. The minor strain relaxation detected, prior to the manual movement, was observed in all tensile tests and is most likely attributable to displacements of the elastic rubber bands within the clamping device.

During destructive tensile tests, cracks in the concrete appeared, resulting in sudden force drops and elongation rises. Figure 8 shows this behavior in a comparable range for both, inner and outer strain gauges. As the force, due to the steadily moving test stand, increases, the device under test experiences more and more mechanical stress. At a certain point, the concrete rips and gives way for a relative movement between the concrete and the basalt reinforcement. This results in an overall elongation of the system, which is measured by the applied strain gauges, shown in Figure 8. During destructive tests, several cracks occur. For a more detailed insight into the destructive strain measurements, only one is shown here.

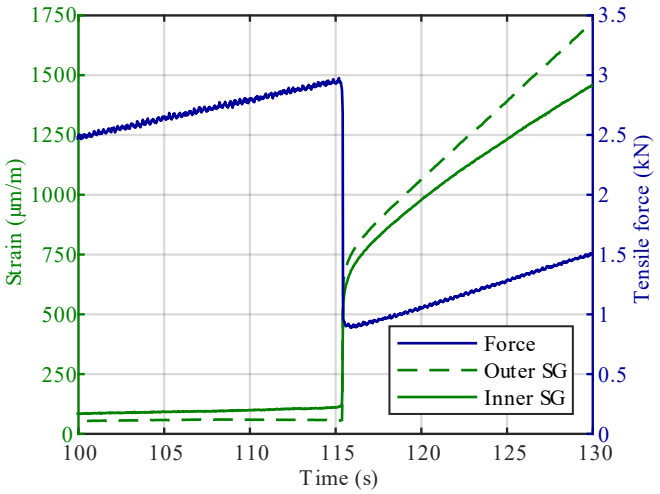

Figure 8. Concrete ripping apart during a destructive tensile test. The applied test stand force, shown in blue, drops due to the formation of a crack. The outer reference strain gauge in dashed green, and the inner steel wire strain gauge (green line) show the feasibility of crack detection. Both measurement signals were recorded with the MX1615B.

4.2 Compression tests

Due to concrete's high compressive strength and previous unreinforced compression tests, a linearly increasing compression force of up to 60 kN was applied for non-destructive test measurements, again less than half of the expected maximum load, as stated in Table 2. Given the significantly higher forces during this measurement session, correspondingly greater changes in the signals were expected to be observed.

Figure 9 illustrates, similar to Figure 7, two separate compressive test measurements with the inner steel wire strain gauge. The compressive force is shown in blue, and the measurement signals from the custom electronics on the left and the MX1615B on the right are shown in green. Both strain signals were again filtered using the FIR low-pass filter with filter length 101 and a cut-off frequency of 2 Hz.

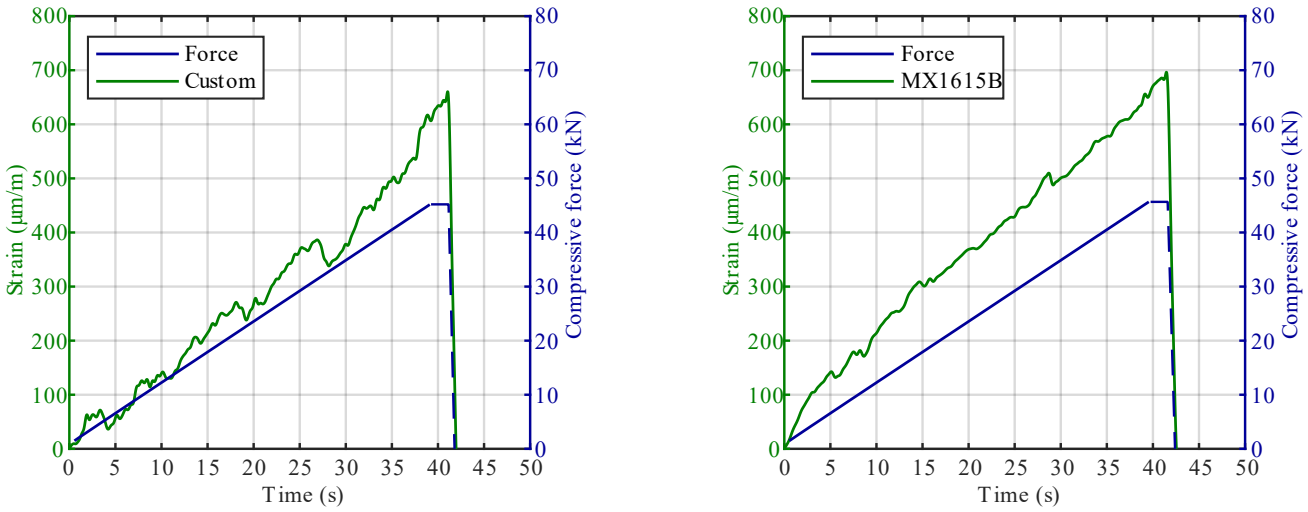

Figure 9. Two non-destructive compressive tests with an in-built hand-made strain gauge in green, measured with the custom-made electronics (left) and with the MX1615B (right). The applied compressive force is shown in blue.

DOI: 10.3217/978-3-99161-057-1-100

Once again, the load was held at a specific point before manually setting it to zero after a few seconds, shown with the dashed blue line. The fluctuations in the strain measurement signals are believed to be a result of relative movement between the individual components of the composite material.

4.3 Evaluation of Noise

During all tests, the Quantum MX1615B (accuracy class 0.1, linearity deviation 0.05) was used alongside the PL-120-11-3LJCT-F and PL-60-11-3LJCT-F strain gauges, which have a gain factor of 2.1 ± 1%. According to the datasheet, the Quantum MX1615B produces less than 0.6 µV/V noise at 25°C with a 5 V excitation.

In comparison, the ADS1261, used in the custom system, exhibits 30 nVRMS noise (gain 128, 20 SPS) and a linearity of 2 ppm. The stranded steel wire used in the setup is assumed to have a gain factor of 2. Throughout the tests, temperature and humidity were maintained constant, as the test stand is located in a sub-terrain basement. These factors lead to the standard deviations of the detrended measurement signals, as shown in Table 3.

Table 3. Standard deviations obtained from the reference Quantum MX1615B and the custom measurement system, both for tensile and compressive tests after low-pass filtering.

Standard deviations	Tensile (µm/m)	Compressive (µm/m)
MX1615B	0.769	0.563
Custom system	1.49	2.07

As is visible, after low-pass filtering, the standard deviations are in the same order of magnitude.

5 CONCLUSION

Our measurements aimed to demonstrate the feasibility of in-built strain gauges into the basalt reinforcement for future automated production processes.

Based on prior tests, tensile as well as compressive tests were conducted, using hand-patterned steel wire strain gauges mounted on basalt reinforcement to measure the device under test's elongation and compression. Both compressive and tensile tests showed promising results. Relative movement between the basalt reinforcement and the concrete is the same for wounded basalt fibers as well as basalt rebar. Furthermore, the adhesion between the hand-patterned strain gauge and the basalt rebar holds and the strain gauges endure the harsh concrete environment without failure, as seen in Figure 2.

These are promising findings for further development of automated basalt reinforcement construction. Additionally, it shows that the adhesion between the reinforcement and the concrete has to be improved in future revisions, giving valuable insight into the dynamic behavior of the compound material.

Our low-cost, custom-made, first prototype measurement device reaches acceptable sensitivity close to the range of the Quantum MX1615B measurement system. As a result, we demonstrated the viability of our low-cost, structural health monitoring concept, feasible for the instrumentation of a whole tunnel.

Future revisions of the electronics anticipate the replacement of the Arduino with an industrial-grade microcontroller, further reduction of component sizes, and the removal of the OLED screen for low-power operations within tunnel segments. Additionally, all metrics for improvement, concerning an integrated solution of both the electronics and sensors for the application in concrete elements, including temperature compensation actions, are being considered. These include half-bridge configurations, degradation compensation, and software measures to counteract false-positive and false-negative readings.

Moving forward, we anticipate further tests including bending beam tests as a precursor to tests on real tunnel segments due to more representative conditions of standard segment test scenarios. Furthermore, in the long term, we propose test arrangements with multiple measurement systems in segments, forming a tunnel ring, for real-world test environments.

USE OF AI TOOLS

The authors acknowledge the use of AI-based grammar tools for language refinement.

ACKNOWLEDGMENTS

The authors gratefully acknowledge the financial support of the Austrian Research Promotion Agency (FFG) through the FFG-funded project "*EbiT – Endlosbasaltfaser als smarte Bewehrung im Tiefbau"* (FO999913255) and the valuable contributions of the project partner Fiber Elements GmbH to this research.

REFERENCES

[1] European Council, Climate change: what the EU is doing, https://www.consilium.europa.eu/en/policies/climate-change/, retrieved March 2025.
[2] UN environment programme, Global status report for buildings and construction, Global Alliance for Buildings and Construction, 2020.
[3] GCCA – Global Cement and Concrete Association, GNR 2.0 – GCCA in Numbers, https://gccassociation.org/sustainability-innovation/gnr-gcca-in-numbers/, 2021.
[4] J.G.J. Olivier, J.A.H.W. Peters, PBL Netherlands Environmental Assessment Agency, Trends in global CO_2 and total greenhouse gas emissions: 2020 Report, PBL publication number: 4331, 2020.
[5] Sauer, J., Ökologische Betrachtungen zur Nachhaltigkeit von Tunnelbauwerken der Verkehrsinfrastruktur, Dissertation, Technische Universität München, Institut für Baustoffe und Konstruktion, Lehrstuhl für Massivbau, 2016.
[6] EURAC RESEARCH, Ausbau Eisenbahnachse München-Verona - Brenner Basistunnel. Bereich Umweltplanung - Erstellung eines CO_2-Haushalts, Untersuchung der Nachhaltigkeit des Brenner Basistunnels im Hinblick auf seine CO_2-Emissionen, Innsbruck, Juni 2011.
[7] Kromoser, B., Reichenbach, S., Stoiber, N., Preinstorfer, P. and Huber, T., Potentiale von nichtmetallischer Bewehrung im Infrastruktur-Betonbau NIMETBEW, Endbericht, Wien: E212-02 - Institut für Tragkonstruktionen - Forschungsbereich Stahlbeton- und Massivbau, https://projekte.ffg.at/anhang/62790e46a3083_NIMETBEW_Ergebnisbericht.pdf, 2022.
[8] DBF - Deutsche Basaltfaser GmbH, Technisches Datenblatt, BF-17/2400, 2024.
[9] M. Egger, Gestickte Bewehrungen für Textilbeton, Dissertation, Universität Innsbruck, urn:nbn:at:at-ubi:1-103523, 2022.
[10] ÖBB-Infrastruktur AG, Netzzustandsbericht 2022 - ÖBB, 2023.
[11] ÖBB-Infrastruktur AG, Regelwerk 06.01.02, Konstruktiver Ingenieurbau: Instandhaltung – Instandhaltungsplan, 2012.
[12] R. Matt, B. Moritz and T. Parapatich, Challenges and New Approaches for the Inspection of Railway Tunnels – Asset Safety Management,

DOI: 10.3217/978-3-99161-057-1-100

Geomechanics and Tunnelling 17, Nr. 5, pages 473–81. https://doi.org/10.1002/geot.202400048.
[13] AMBITION - Entwicklung eines integrativen Ansatzes zur Messung und Bewertung von Eisenbahn- und Straßentunnel, Ergebnisbericht. Ein Projekt finanziert im Rahmen der Pilotinitiative Verkehrsinfrastrukturforschung 2015, BMK, FFG, https://projekte.ffg.at/anhang/5dd541860bcd3_VIF2015_AMBITION-Ergebnisbericht.pdf, 2018.
[14] K. Bergmeister, U. Santa, and A. Strauss, Überwachung und Analyse der Lebensdauer von Tunnelbauwerken, Beton- und Stahlbetonbau 102, Nr. 1, pages 24–32, https://doi.org/10.1002/best.200600528, 2007.
[15] Ł. Bednarski, R. Sieńko, T. Howiacki, and K. Zuziak, The Smart Nervous System for Cracked Concrete Structures: Theory, Design, Research, and Field Proof of Monolithic DFOS-Based Sensors, Sensors 22, Nr. 22, https://doi.org/10.3390/s22228713, 2022.
[16] C. Monsberger, W. Lienhart, In-situ Deformation Monitoring of Tunnel Segments using High-resolution Distributed Fibre Optic Sensing, The 8th International Conference on Structural Health Monitoring of Intelligent Infrastructure, 2017.
[17] T. Quadflieg, O. Stolyarov, and T. Gries, Carbonfaserbewehrung als Sensor für Bauwerke, Beton- und Stahlbetonbau, 112(8), pages 541-544, 2017.
[18] P. Bajpai, Biermann's Handbook of Pulp and Paper - Process Control, pages 483–492, doi:10.1016/B978-0-12-814238-7.00024-6, 2018.
[19] W. Bolton, Control Systems, pages 1–36, doi:10.1016/b978-075065461-6/50001-5, 2002.
[20] Bekaert, Bekinox VN, https://api.bekaert.cn/media/wysiwyg/files/basic_materials/CD035_Datasheet-VN-Bekiflex.pdf, retrieved March 2025.
[21] DBF - Deutsche Basaltfaser GmbH, Technisches Datenblatt, Basalt Rebar, 2024.
[22] ALTHEN Mess- & Sensortechnik GmbH, P-Series - Polyester Strain Gauges, https://www.althensensors.com/uploads/products/datasheets/plc-series-polyester-backing-wire-straingauge-for-concrete-material-en.pdf, retrieved March 2025, 2021.
[23] Texas Instruments, ADS1261 ADC, https://www.ti.com/product/de-de/ADS1261, retrieved March 2025.
[24] Arduino S.r.l., Arduino Uno, https://store.arduino.cc/en-at/products/uno-r4-minima, retrieved March 2025.
[25] HBK, Quantum MX1615B, Data Sheet, https://www.hbm.com/fileadmin/mediapool/hbmdoc/technical/B03899.pdf, retrieved March 2025, 2023.